Electronic Supplementary Material (ESI) for Journal of Materials Chemistry A.
This journal is © The Royal Society of Chemistry 2020

Electronic Supplementary Information (ESI) for

A knot-linker planarity control for constructing highly crystalline cationic covalent organic frameworks: decoding the effect of crystallinity on adsorption performance

Hong-Ju Da,[a] Cheng-Xiong Yang*,[a] Hai-Long Qian,[b] and Xiu-Ping Yan*,[b]

[a] Research Center for Analytical Sciences, Tianjin Key Laboratory of Molecular Recognition and Biosensing, College of Chemistry, Nankai University, Tianjin 300071, China

[b] State Key Laboratory of Food Science and Technology, International Joint Laboratory on Food Safety, Institute of Analytical Food Safety, School of Food Science and Technology, Jiangnan University, Wuxi 214122, China

Email: xpyan@jiangnan.edu.cn

Contents

Supplementary Methods

Supplementary Figures

Supplementary Tables

Supplementary Methods

Chemicals and materials. All chemicals used were at least of analytical grade. Guanidine hydrochloride, 2,3-dichlorophenol (2,3-DCP), 2,4-dichlorophenol (2,4-DCP), 2,6-dichlorophenol (2,6-DCP), 3-chlorophenol, 4-chlorophenol and 1-naphthol were bought from Aladdin Chemistry Co. Ltd (Shanghai, China). Hydrazine hydrate (80 wt.%) was purchased from Jiuding Chemical Technology Co. Ltd (Shanghai, China). 2,4,6-Tris(4-formylphenyl)-1,3,5-triazine (TFPT) was obtained from Yahong Biological Technology Co., Ltd (Nanjing, China). 1,3,5-Tris(4-formylphenyl) benzene (TFPB) and tris(4-formylphenyl) amide (TFPA) were bought from Tongchuangyuan Pharmaceutical Technology Co., Ltd. (Chengdu, China). Tetrahydrofuran (THF), 1,4-dioxane, *N*-methyl pyrrolidone (NMP), *N,N*-dimethyl-acetamide (DMAc), *N,N*-dimethyl-formamide (DMF), methanol (MeOH), ethanol (EtOH), isopropanol (IPA), acetonitrile (ACN) and acetic acid (HAc) were purchased from Concord Fine Chemical Research Institute (Tianjin, China). 2,4-Diclorophenol (2,4-DCP), $CaCl_2$ and $MgSO_4$ were obtained from Guangfu Fine Chemical Research Institute (Tianjin, China). Sodium chloride (NaCl) was purchased from Tianjin Benchmark Chemical Reagent Co. Ltd (Tianjin, China). Ultrapure water was obtained from Wahaha Foods Co. Ltd (Tianjin, China). River water sample was collected from Weijin River. Lake water sample was gathered from Xinkai Lake.

Characterization. A Nicolet AVATAR-360 spectrometer (Nicolet, USA) was used to record the Fourier transform infrared (FT-IR) spectra from 4000 to 400 cm^{-1} using

KBr as support. The powder X-ray diffraction (PXRD) data were collected on a D/max-2500 diffractometer (Rigaku, Japan) equipped with Cu K_α (λ = 1.5418 Å) from 3° to 40° at a step size of 0.02^o and a scanning speed of 8° min^{-1}. The solid state ^{13}C nuclear magnetic resonance (NMR) was measured on Infinity plus 400 (VARIAN, USA) under the ^{13}C CP-MAS model. The scanning electronic microscopy (SEM) images and energy-dispersive X-ray spectroscopy (EDX) elements mapping were obtained from a JSM7500F field (JEOL, Japan). The X-ray photoelectron spectroscopy (XPS) of synthesized iCOFs was measured on an Axis Ultra DLD (Kratos, Britain) system equipped with a monochromated Al Kα X-ray source (hν = 1486.6 eV) and delay line detector (Kratos, Manchester, UK). The high resolution transmission electron microscopy (TEM) images were measured on a FEI Talos F200XG2 transmission electron microscope (FEI, Czech) under an accelerating voltage of 200 kV by dropping samples on super-thin carbon films. The N_2 adsorption isotherms were recorded on an ASAP 2020 micropore physisorption analyzer (Micromeritics, USA) at 77 K with the desorption temperature of 150 ^oC. The nonlocal density functional theory (NLDFT) was adopted to analyze the pore size distribution. The concentration of 2,4-DCP was determined on a high-performance liquid chromatography (HPLC, Waters 510, USA) pump with Waters 486 UV detector using Baseline ODS column (25 cm long × 4.6 mm i.d., Tianjin, China). The pH values were measured on a PHS-3E Acidometer (Youke, China).

Synthesis of TFPB-TG_{Cl}-iCOF. The synthetic process of TFPB-TG_{Cl}-iCOF was

similar to that of TFPT-TG_{Cl}-iCOF. The TG_{Cl} and TFPB were dispersed in a binary solvent consisting of diverse volume ratios of water/3 mol L^{-1} HAc/6 mol L^{-1} HAc and organic solvents (1,4-dioxane, THF, DMAc or NMP). Firstly, dispersing TG_{Cl} (7.03 mg, 0.05 mmol) and TFPB (19.5 mg, 0.05 mmol) in 1.0 mL of binary solvent in a 20 cm long × 8 mm i.d glass tube. After three freeze-pump-thaw cycles, the glass tube was sealed and placed in an oven at 120 ^{o}C for 3 days. The products were filtrated out and Soxhlet extracted by DMF and MeOH for 48 h, respectively. Finally, the obtained light-yellow powder was dried under vacuum with the yield of 86%. Anal. Cald. for $(C_{28}H_{21}N_6Cl)_n$ (%): C 70.51; H 4.41; N 17.63; Cl 7.45. Found (%): C 66.07; H 4.11; N 15.43; Cl 6.71. FT-IR: 3431, 2921, 2851, 1659, 1630, 1598, 1573, 1514, 1411, 1363, 1298, 1100, 1059, 811, 756, 662 cm^{-1}. PXRD: 5.9^{o}, 10.5^{o}, 22.8^{o}.

Synthesis of TFPA-TG_{Cl}-iCOF. The synthetic process of TFPA-TG_{Cl}-iCOF was similar to that of TFPT-TG_{Cl}-iCOF. The TG_{Cl} and TFPB were dispersed in a binary solvent consisting of diverse volume ratios of water/3 mol L^{-1} HAc/6 mol L^{-1} HAc and organic solvents (1,4-dioxane, THF, DMAc or NMP). Firstly, TG_{Cl} (7.03 mg, 0.05 mmol) and TFPA (16.5 mg, 0.05 mmol) were dispersed in 1.0 mL of binary solvent in a 20 cm long × 8 mm i.d glass tube. After three freeze-pump-thaw cycles, the glass tube was sealed and placed in an oven at 120 ^{o}C for 3 days. The products were filtrated out and Soxhlet extracted by DMF and MeOH for 48 h, respectively. Finally, the obtained dark-yellow powder was dried under vacuum with the yield of 88%. Anal. Cald. for $(C_{22}H_{18}N_7Cl)_n$ (%): C 63.54; H 4.33; N 23.59; Cl 8.54. Found (%): C 58.94; H 3.48; N

22.33; Cl 7.61. FT-IR: 3431, 2921, 2851, 1659, 1630, 1598, 1573, 1515, 1411, 1364, 1299, 1101. 1060, 812, 756, 663 cm^{-1}. PXRD: 21.2^{o}.

DFT simulation of planarity modulators and simulated compounds. The planarity modulators involving TFPT, TFPB, TFPA and simulated compounds including TFPT-G, TFPB-G, TFPA-G for TFPT-TG_{Cl}-iCOF, TFPB-TG_{Cl}-iCOF and TFPA-TG_{Cl}-iCOF were constructed by Material Studio (ver. 2017). The structure optimization of above structures was then calculated in Gaussian 09 by using B3LYP functional and 6-31G basis set.[S1-S3] The dihedral angles of fused phenyl groups to core plane were measured by GaussView 6.0 to demonstrate the specific planarity of different units.

Calculation of stacking energy of iCOFs. The single-layer and bilayer hexagonal units of three iCOFs capped with phenyl groups were constructed by Material Studio (ver. 2017) and then imported into Gaussian 09 for further operations. The distance between two single-layer units was scanned from 5 Å to 3 Å to minimize the energy of structures. The structural optimization was carried out by using PBE functional and the 6-31G basis set.[S4] The single point energy of single-layer and bilayer structures were calculated and SCF energies was corrected with DFT-D (3) correction.[S5] The stacking energies of iCOFs were calculated by the equation of $E_{\text{stacking energy}} = E_{\text{bilayer}} - 2 \times E_{\text{single layer}}$ according to the previous research[S6].

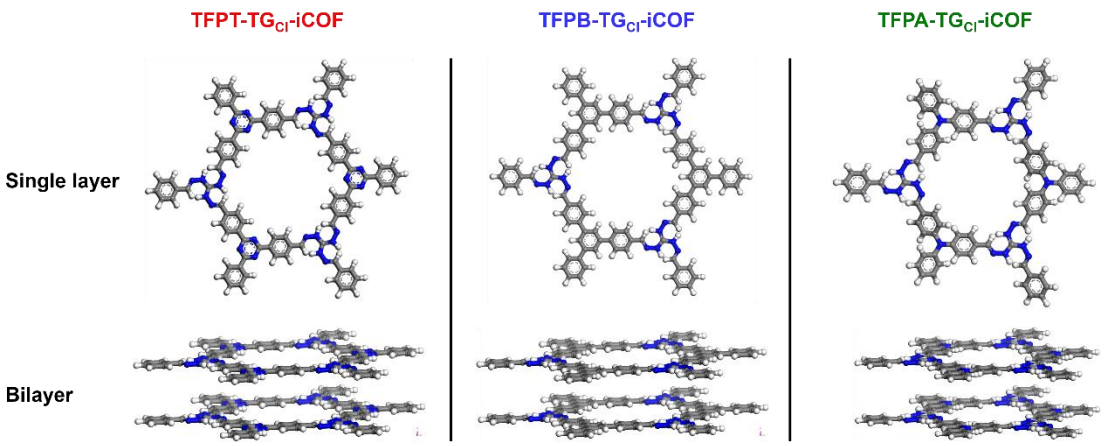

Note: The cationic charges cannot be recognized by Material studio and the extra hydrogen atom of the cationic site in TG_{Cl} obviously disturbs the planarity of layers within iCOFs. Hence, we initially constructed the original structures in Material studio and imported these structures in Gaussian software for further structural optimization. The charge number of a single-layer hexagonal unit was set as three. (C: gray, N: blue, H: white, Cl: green)

Hydrolytic stability studies. Hydrolytic stability of TFPT-TG_{Cl}-iCOF was tested under different pH conditions. The pH values of aqueous solutions were adjusted by 0.1 mmol L^{-1} HCl or 0.1 mmol L^{-1} NaOH. 10 mg of TFPT-TG_{Cl}-iCOF was immersed in 10 mL of aqueous solutions with different pH values (2-10) for 72 h at 25 ^{o}C. The treated TFPT-TG_{Cl}-iCOF were collected, dried and characterized by PXRD.

Effect of pH. 1 mg of TFPT-TG_{Cl}-iCOF was immersed in 1 mL of 2,4-DCP solutions (200 mg L^{-1}) with diverse pH values (2-10) for 1 h. The suspensions were then filtrated by 0.22 µm PES filters. The concentrations of residual 2,4-DCP in the filtrate were determined by HPLC.

Effect of ion strength. The 2,4-DCP solutions (200 mg L^{-1}) with 0.01-1.0 mol L^{-1}

of NaCl, $CaCl_2$ and $MgSO_4$ were prepared to explore the influence of ion strength during the adsorption process. 1 mg of TFPT-TG_{Cl}-iCOF was immersed in 1 mL above solutions for 1 h. After filtrating by 0.22 μm PES filters, the residual concentrations of 2,4-DCP in the filtrate were measured by HPLC.

Effect of humid acid. The 2,4-DCP solutions (200 mg L^{-1}) with different amount of humid acid (1-50 mg L^{-1}) were prepared to study the effect of humid acid (HA) on the adsorption performance of adsorbents. 1 mg TFPT-TG_{Cl}-iCOF was immersed in 1 mL of HA-contained 2,4-DCP solutions for 1 h. After filtrating by 0.22 μm PES filters, the residual concentrations of 2,4-DCP in the filtrate were measured by HPLC.

Desorption experiments. The 2,4-DCP pre-adsorbed TFPT-TG_{Cl}-iCOF was prepared by suspending 60 mg TFPT-TG_{Cl}-iCOF in 60 mL 2,4-DCP (100 mg L^{-1}) for 30 min in a 100 mL round bottom flask. Then, 1 mg 2,4-DCP pre-adsorbed TFPT-TG_{Cl}-iCOF was treated with 1 mL different eluents (MeOH, EtOH, IPA or ACN) under ultrasonication for 10 min. The adsorbent was collected by centrifugation at 8000 rpm for 5 min. The supernatant was filtrated by 0.22 μm PES filters and then determined by HPLC. The elution time (1-10 min) and elution number (1-4) were further optimized by using EtOH as the eluent.

Reusability. The used TFPT-TG_{Cl}-iCOF was washed with EtOH for several times and dried for reusability investigation. 1 mg of regenerated TFPT-TG_{Cl}-iCOF was dispersed in 1 mL of 2,4-DCP (100 mg L^{-1}). After contacting for 30 min at 25 °C, the adsorbent was collected by centrifugation at 8000 rpm for 5 min. The residual concentrations of 2,4-DCP in the supernatant were measured by HPLC. The collected

TFPT-TG_{Cl}-iCOF was used for the next desorption process. The adsorption-desorption cycles were repeated according to above procedures for 4 times.

Adsorption of 2,4-DCP from real water samples. The practical water samples were prepared by diluting the stock solutions (2000 mg L^{-1}) of 2,4-DCP with the river, lake and tap water to the final concentrations of 200 mg L^{-1}. 1 mg of TFPT-TG_{Cl}-iCOF was dispersed in 1.0 mL of above prepared real water samples. After contacting for 1 h at 25 °C, the mixtures were filtrated with 0.22 μm PES filters. The residual concentrations of 2,4-DCP were determined by HPLC.

Adsorption kinetics. The pseudo-second-order kinetic model is shown as equations S1 and S2. Where q_t is the adsorption capacity (mg g^{-1}) at a predetermined time t (min) and q_e is the equilibrium adsorption capacity (mg g^{-1}). k_2 is the rate constant of pseudo-second-order model (g mg^{-1} min^{-1}):

$$\frac{dq_t}{dt} = k_2(q_e - q_t)^2 \quad \text{(S1)}$$

$$\frac{t}{q_t} = \frac{1}{k_2 q_e^2} + \frac{t}{q_e} \quad \text{(S2)}$$

The pseudo-first-order kinetic model is expressed as equation S3. Where q_t and q_e are the adsorption capacity (mg g^{-1}) at a certain time t (min) and equilibrium, respectively, and k_1 is the rate constant for the pseudo-first-order model.

$$\ln(q_e - q_t) = \ln q_e - k_1 t \quad \text{(S3)}$$

Adsorption isotherms. The Langmuir adsorption model implies that the adsorption behavior is monolayer sorption on a homogenous surface. The Langmuir adsorption model is expressed as equation S4. Where q_0 (mg g^{-1}) is the maximum

adsorption capacity. q_e (mg g^{-1}) is the equilibrium adsorption capacity. Ce (mg L^{-1}) is the equilibrium concentration of 2,4-DCP. b (L mg^{-1}) is the Langmuir constant.

$$\frac{c_e}{q_e} = \frac{1}{q_0 b} + \frac{c_e}{q_0} \quad \text{(S4)}$$

The Freundlich model is raised based on the heterogeneous sorption process. The Freundlich model is given as equation S5. Where q_e (mg g^{-1}) is the equilibrium adsorption capacity. C_e (mg L^{-1}) is the concentration of 2,4-DCP at equilibrium, K_F [(mg g^{-1})/ (mg L^{-1}) (1/n)] is the Freundlich affinity coefficient.

$$\ln q_e = \ln k_F + \frac{1}{n}\ln c_e \quad \text{(S5)}$$

Calculation of thermodynamic parameters. The thermodynamic parameters were calculated based on the following equations:

$$K_0 = \frac{q_e}{c_e} \quad \text{(S6)}$$

$$\Delta G = -RT\ln K_0 \quad \text{(S7)}$$

$$\ln K_0 = \frac{\Delta S}{R} - \frac{\Delta H}{RT} \quad \text{(S8)}$$

Where q_e (mg g^{-1}) is the equilibrium adsorption capacity, C_e (mg L^{-1}) is the equilibrium concentration, R is the universal gas constant (8.314 J mol^{-1} K^{-1}). The thermodynamic parameters those need to be calculated include enthalpy change (ΔH, kJ mol^{-1}), free energy change (ΔG, kJ mol^{-1}), entropy change (ΔS, J mol^{-1} K^{-1}) and the thermodynamic equilibrium constant (K_0). K_0 can be obtained from the intercept by plotting ln (q_e/C_e) against qe. ΔH and ΔS were obtained from the slope and intercept by plotting ln K_0 against 1/T.

Supplementary Figures

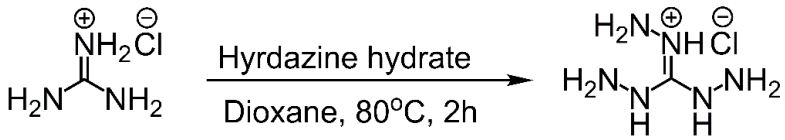

Figure S1. Scheme for the synthesis of TG_{Cl}.

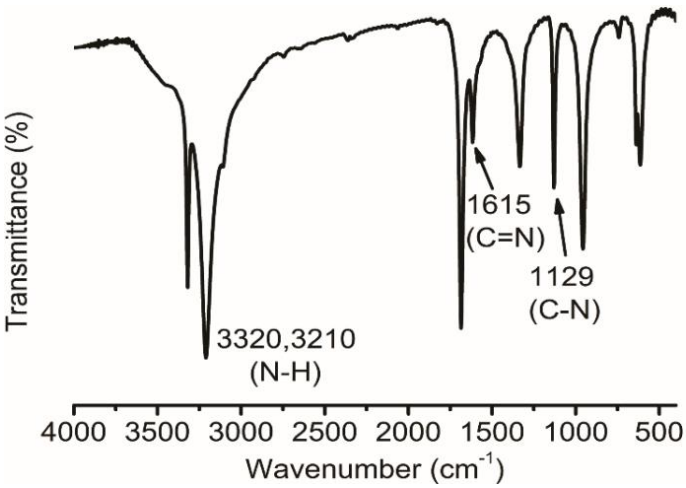

Figure S2. FT-IR spectrum of the synthesized TG_{Cl}.

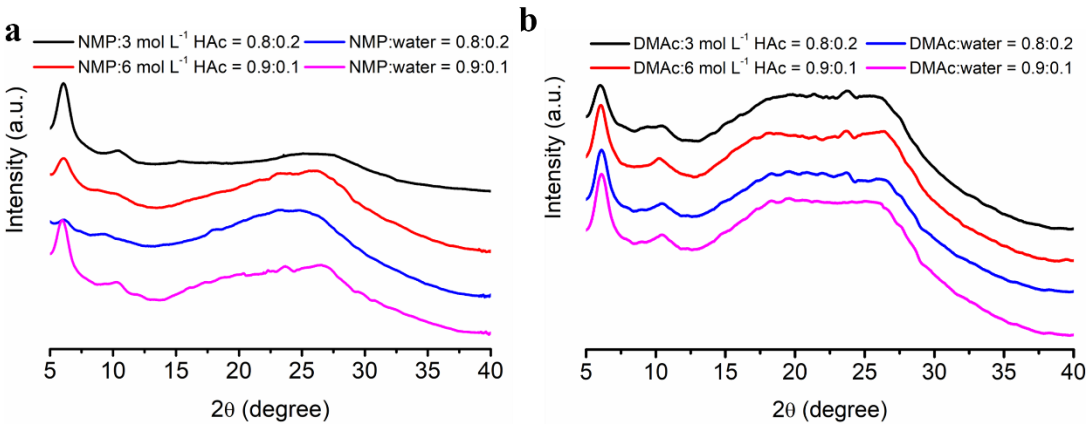

Figure S3. Effect of solvent composition on the synthesis of TFPT-TG_{Cl}-iCOF: (a) NMP/water; (b) DMAc/water. High-crystalline TFPT-TG_{Cl}-iCOF was successfully obtained by using NMP/3 mol L^{-1} acetic acid (HAc) (v/v, 0.8:0.2) at 120 ^{o}C for 3 days.

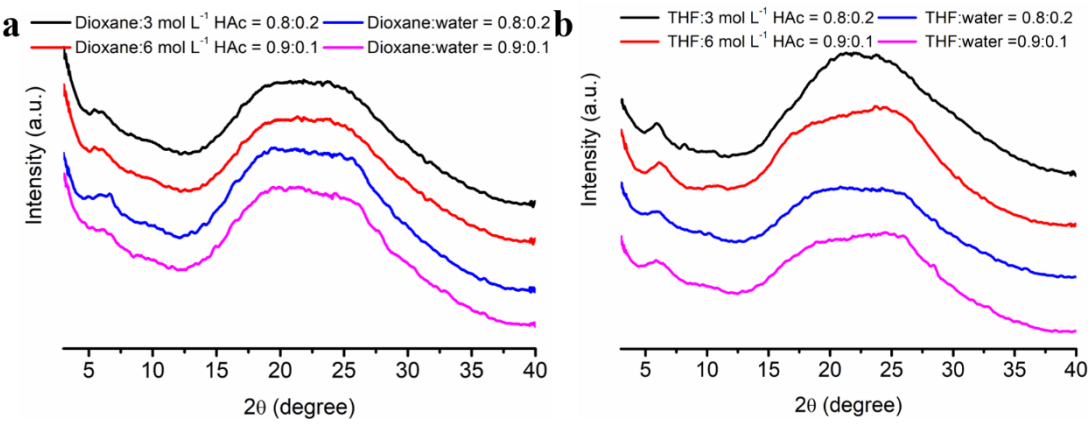

Figure S4. Effect of solvent composition on the synthesis of TFPB-TG_{Cl}-iCOF: (a) 1,4-dioxane/water; (b) THF/water. The PXRD patterns of gel-like products in DMAc/water and NMP/water were hard to collect. THF/3 mol L^{-1} HAc (v/v, 0.8:0.2) was selected as optimal solvent.

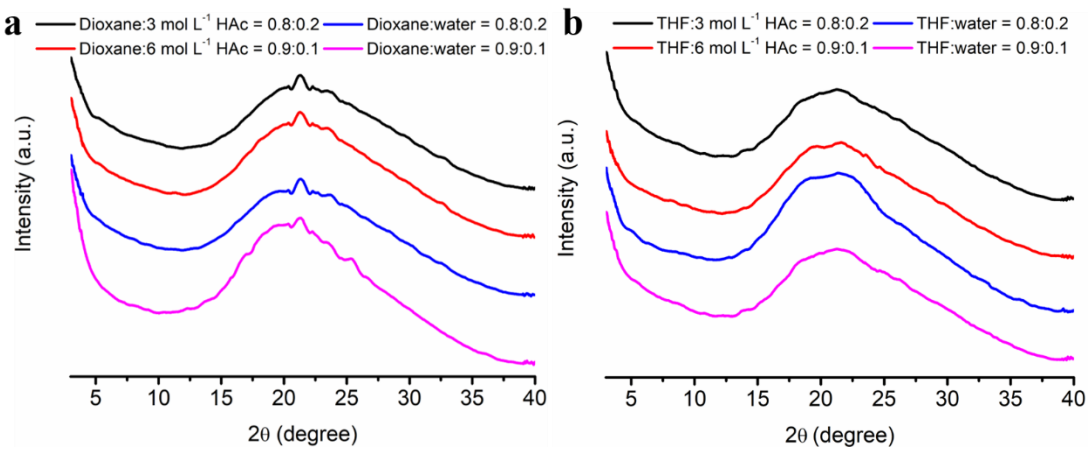

Figure S5. Effect of solvent composition on the synthesis of TFPA-TG_{Cl}-iCOF: (a) Dioxane/water; (b) THF/water. The PXRD patterns of the gel-like products in DMAc/water and NMP/water were hard to collect. The solvent was selected as THF/3 mol L^{-1} HAc (v/v, 0.8:0.2).

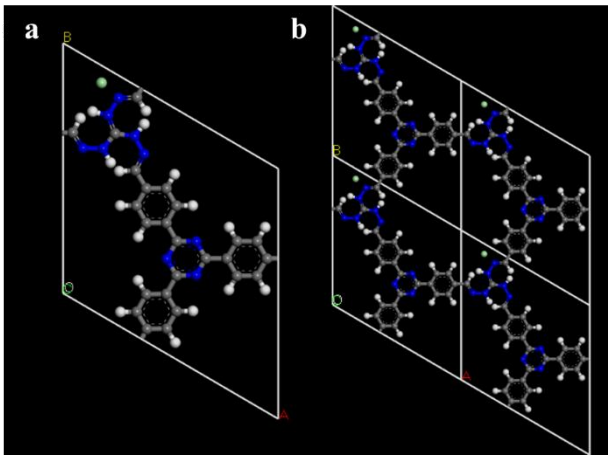

Figure S6. (a) Unit cell and (b) slipped crystal lattice of TFPT-TG_{Cl}-iCOF. C: gray; N: blue; Cl: green; H: white.

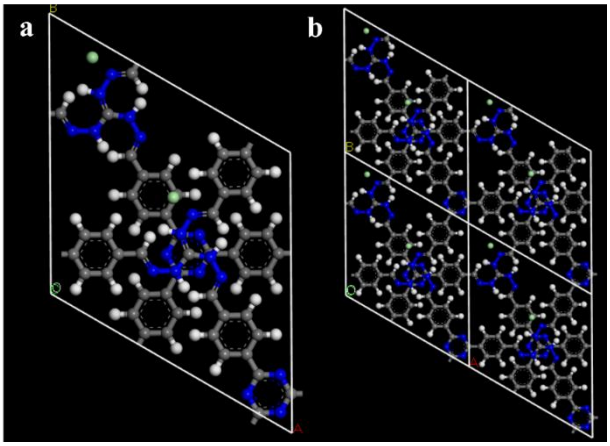

Figure S7. (a) Unit cell and (b) staggered crystal lattice of TFPT-TG_{Cl}-iCOF. C: gray; N: blue; Cl: green; H: white.

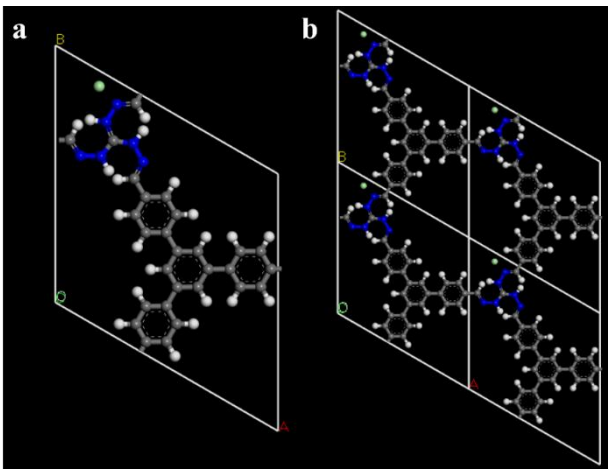

Figure S8. (a) Unit cell and (b) slipped crystal lattice of TFPB-TG_{Cl}-iCOF. C: gray; N: blue; Cl: green; H: white.

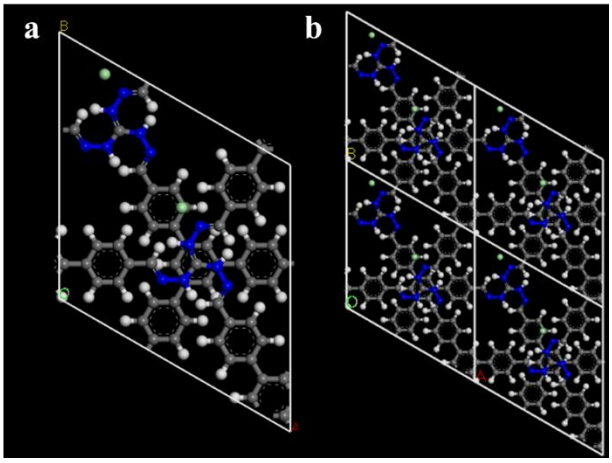

Figure S9. (a) Unit cell and (b) staggered crystal lattice of TFPB-TG_{Cl}-iCOF. C: gray; N: blue; Cl: green; H: white.

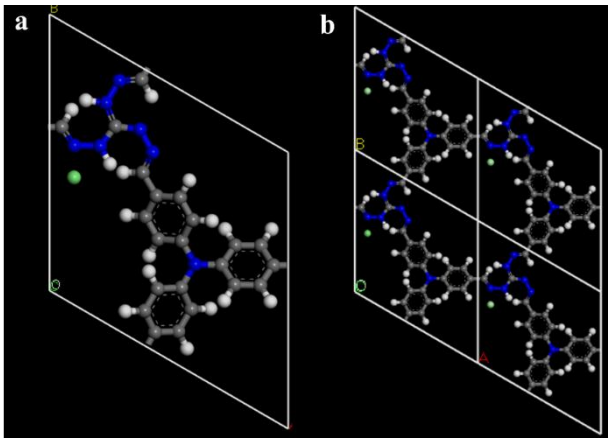

Figure S10. (a) Unit cell and (b) slipped crystal lattice of TFPA-TG_{Cl}-iCOF. C: gray; N: blue; Cl: green; H: white.

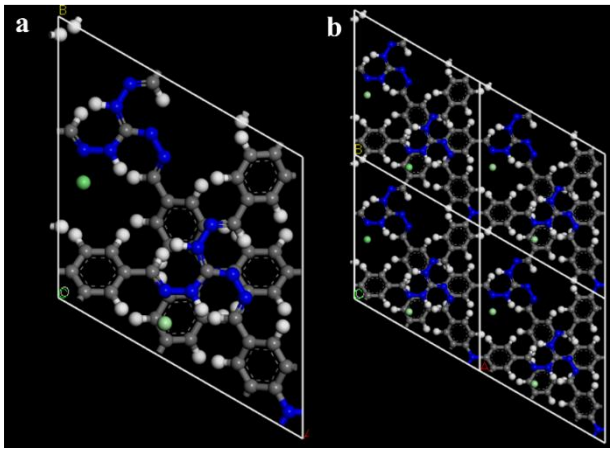

Figure S11. (a) Unit cell and (b) staggered crystal lattice of TFPA-TG_{Cl}-iCOF. C: gray; N: blue; Cl: green; H: white.

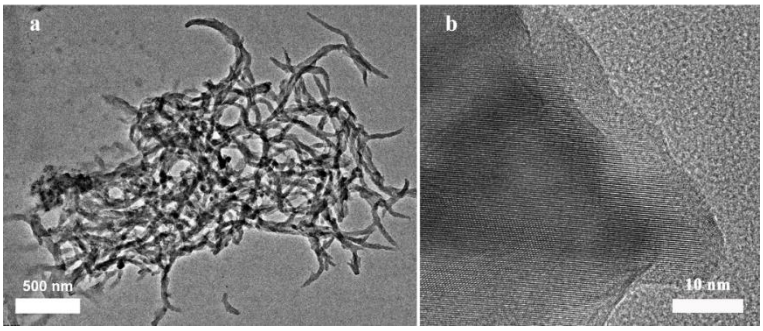

Figure S12. TEM images of the as-synthesized TFPT-TG_{Cl}-iCOF. A wide range of ordered lattice structure was observed in TEM image.

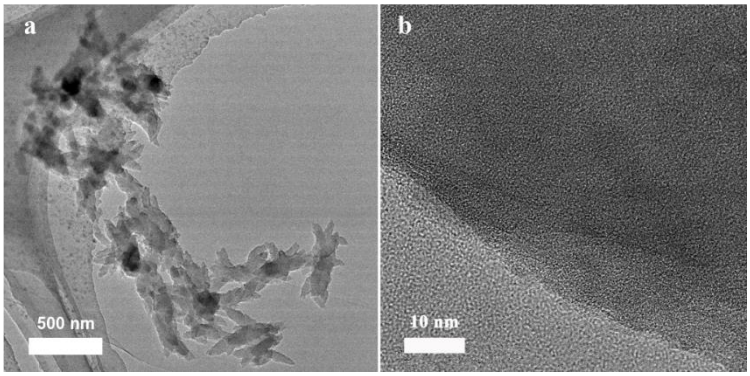

Figure S13. TEM images of the as-synthesized TFPB-TG_{Cl}-iCOF. The ordered structure was only observed at the edge of TFPB-TG_{Cl}-iCOF.

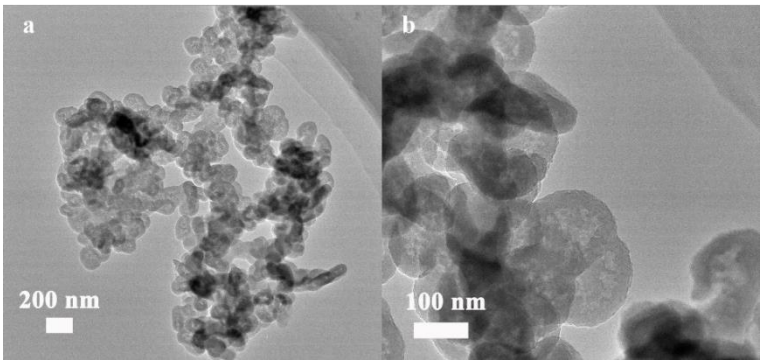

Figure S14. TEM images of the as-synthesized TFPA-TG_{Cl}-iCOF. Non-crystalline structure shows the hollow sphere morphology.

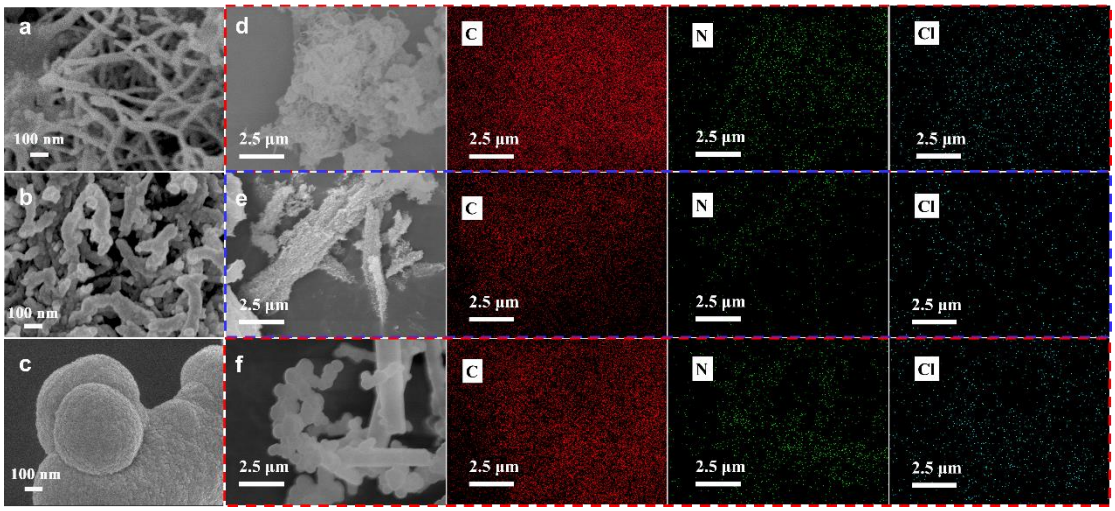

Figure S15. SEM images of (a) TFPT-TG_{Cl}-iCOF, (b) TFPB-TG_{Cl}-iCOF and (c) TFPA-TG_{Cl}-iCOF and EDX mapping images of (d) TFPT-TG_{Cl}-iCOF, (e) TFPB-TG_{Cl}-iCOF and (f) TFPA-TG_{Cl}-iCOF, including elements C, N, and Cl.

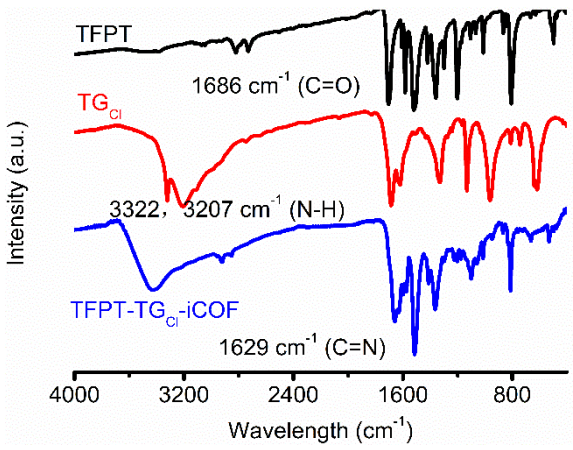

Figure S16. FT-IR spectra of TFPT, TG_{Cl} and TFPT-TG_{Cl}-iCOF.

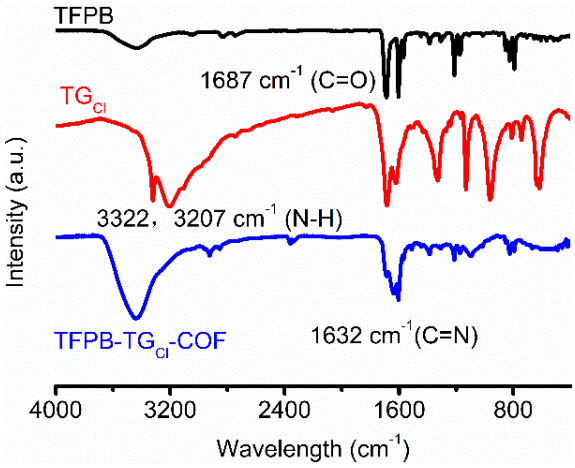

Figure S17. FT-IR spectra of TFPB, TG_{Cl} and TFPB-TG_{Cl}-iCOF.

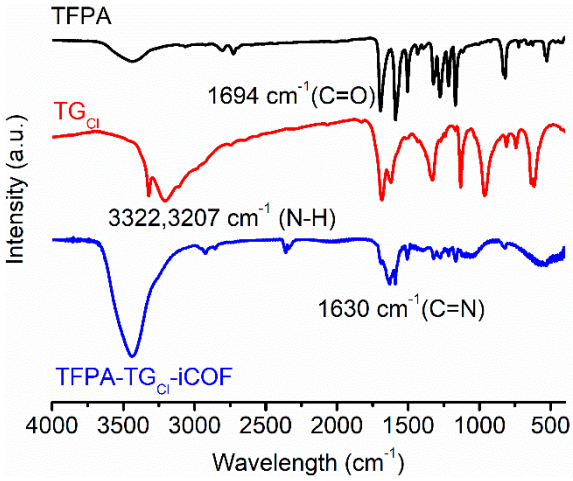

Figure S18. FT-IR spectra of TFPA, TG_{Cl} and TFPA-TG_{Cl}-iCOF.

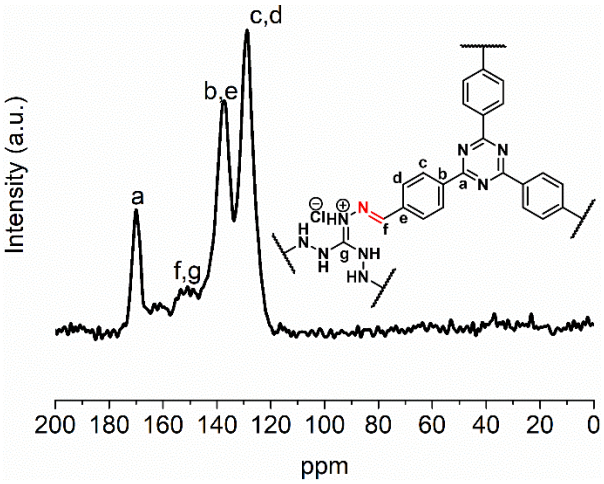

Serial number	Chemical shift (ppm)
a	170
b	137
c	127
d	129
e	133
f	155
g	152

Figure S19. Solid ^{13}C NMR spectrum and peak contribution for TFPT-TG$_{Cl}$-iCOF.

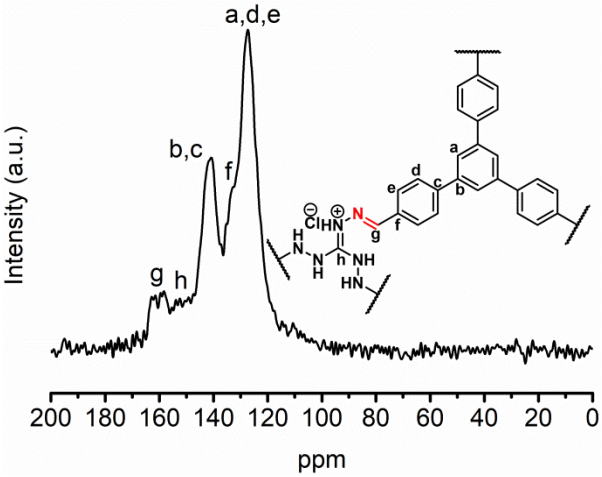

Serial number	Chemical shift (ppm)
a	125
b	137
c	143
d	128
e	129
f	133
g	158
h	152

Figure S20. Solid ^{13}C NMR spectrum and peak contribution for TFPB-TG$_{Cl}$-iCOF.

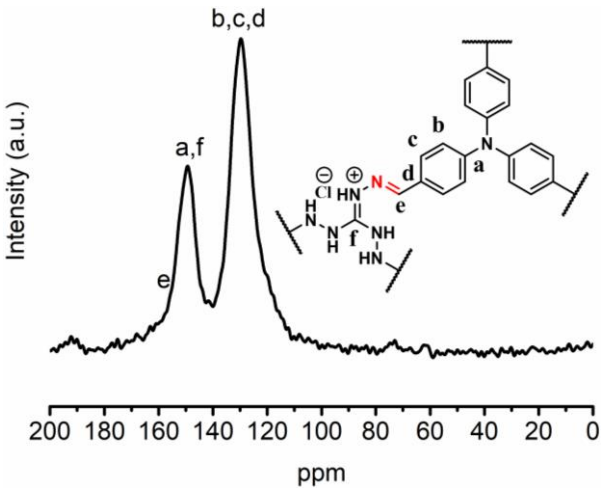

Serial number	Chemical shift (ppm)
a	148
b	125
c	129
d	128
e	156
f	152

Figure S21. Solid ^{13}C NMR spectrum and peak contribution for TFPA-TG$_{Cl}$-iCOF.

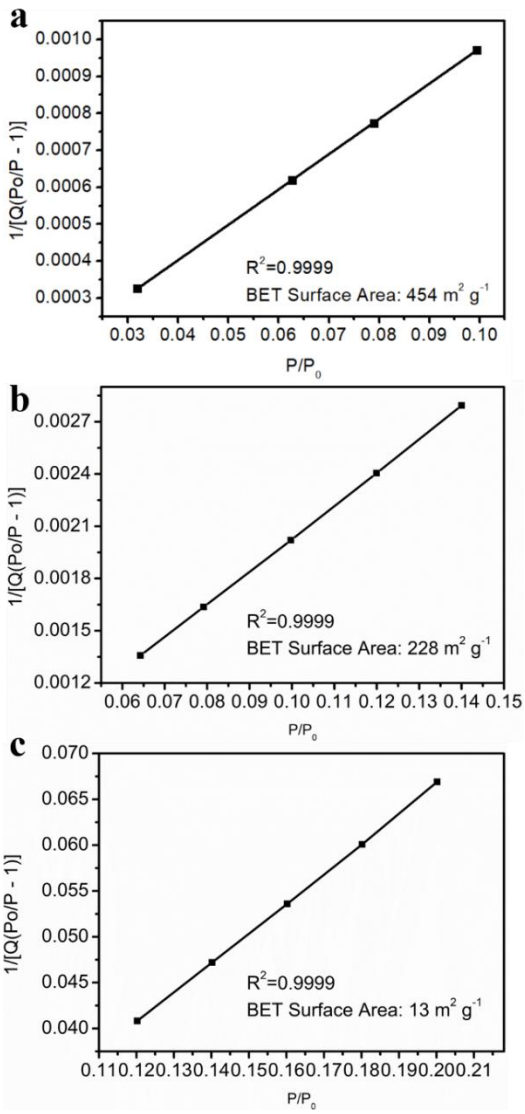

Figure S22. BET surface area plots calculated from the N_2 adsorption-desorption isotherms: (a) TFPT-TG_{Cl}-iCOF; (b) TFPB-TG_{Cl}-iCOF; (c) TFPA-TG_{Cl}-iCOF.

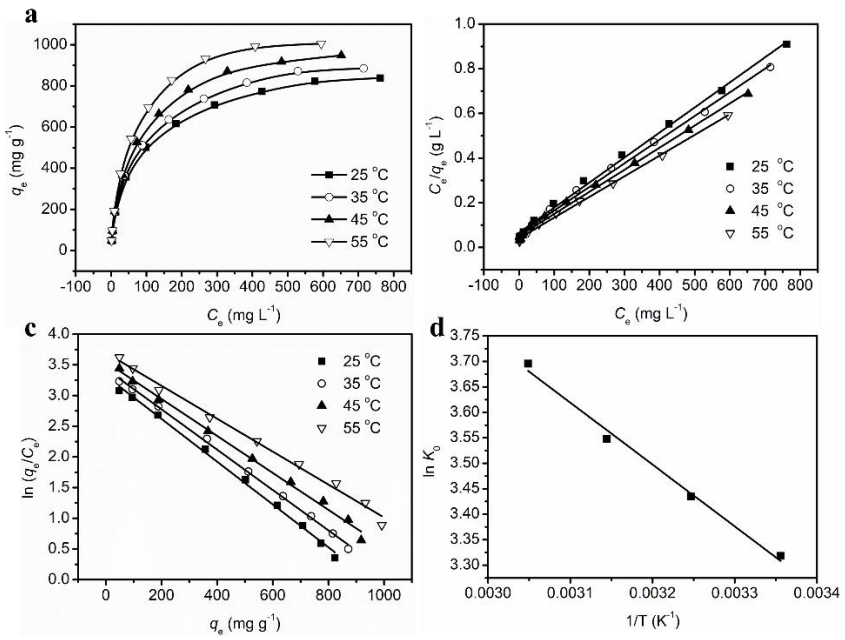

Figure S23. (a) Adsorption isotherms of 2,4-DCP on TFPT-TG$_{Cl}$-iCOF. (b) Plots of C_e/q_e against C_e for Langmuir model; (c) ln (q_e/C_e) against q_e at different temperatures; (d) plot of lnK_0 vs. 1/T for the adsorption of 2,4-DCP on TFPT-TG$_{Cl}$-iCOF.

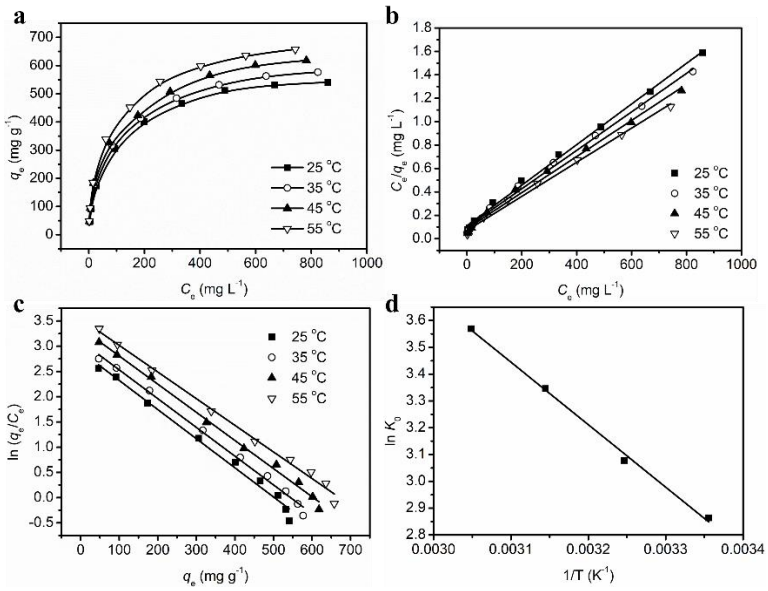

Figure S24. (a) Adsorption isotherms of 2,4-DCP on TFPB-TG$_{Cl}$-iCOF. (b) Plots of C_e/q_e against C_e for Langmuir model; (c) ln (q_e/C_e) against q_e at different temperatures; (d) plot of lnK_0 vs. 1/T for the adsorption of 2,4-DCP on TFPB-TG$_{Cl}$-iCOF.

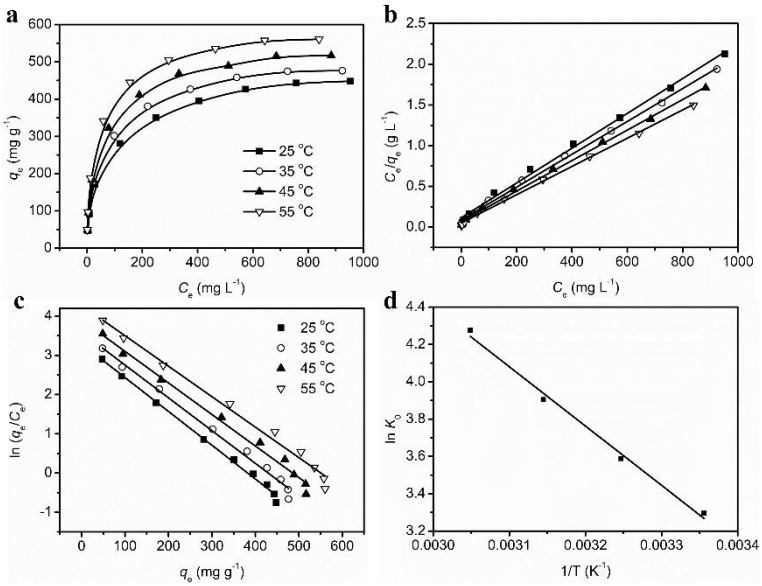

Figure S25. (a) Adsorption isotherms of 2,4-DCP on TFPA-TG$_{Cl}$-iCOF. (b) Plots of C_e/q_e against C_e for Langmuir model; (c) ln (C_e/q_e) against C_e at different temperatures; (d) plot of lnK_0 vs. 1/T for the adsorption of 2,4-DCP on TFPA-TG$_{Cl}$-iCOF.

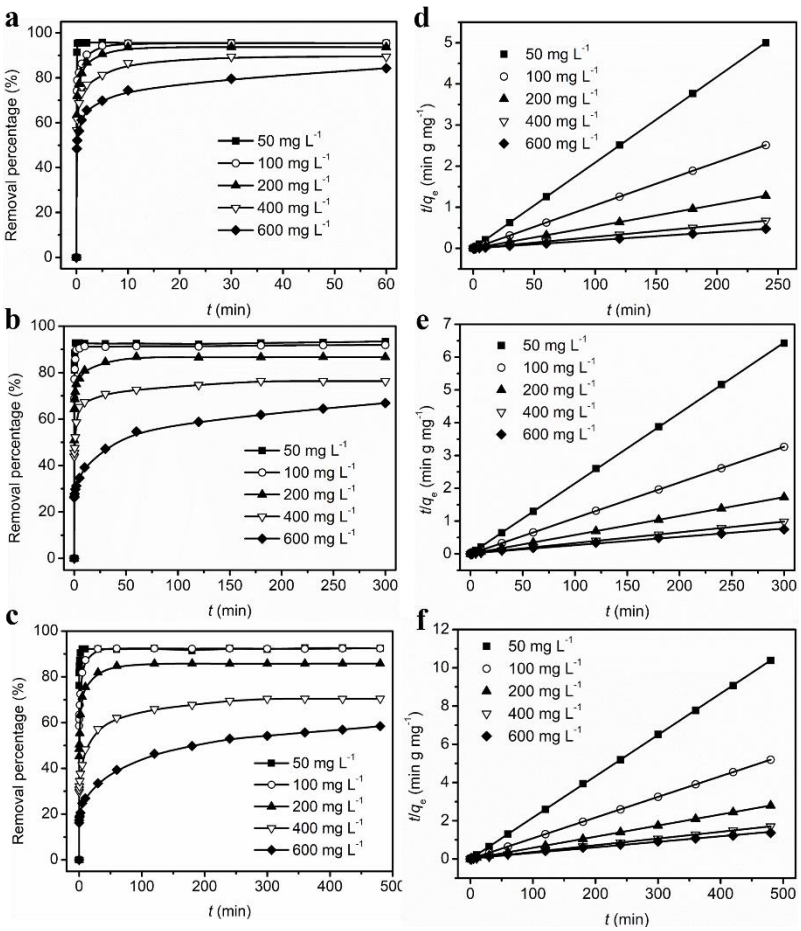

Figure S26. Time-dependent adsorption of 2,4-DCP on iCOFs at 298 K: (a) TFPT-TG_{Cl}-iCOF; (b) TFPB-TG_{Cl}-iCOF; (c) TFPA-TG_{Cl}-iCOF; and their corresponding Pseudo-second-order kinetics adsorption plots: (d) TFPT-TG_{Cl}-iCOF; (e) TFPB-TG_{Cl}-iCOF; (f) TFPA-TG_{Cl}-iCOF.

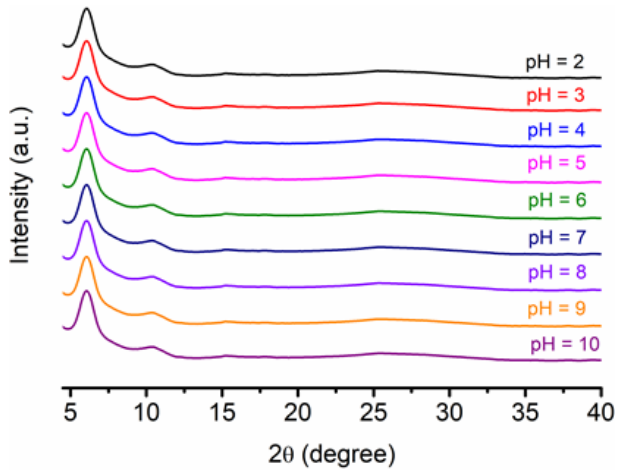

Figure S27. PXRD patterns of TFPT-TG$_{Cl}$-iCOF after immersing in aqueous solutions with different pHs at 25 ^{o}C for 3 days.

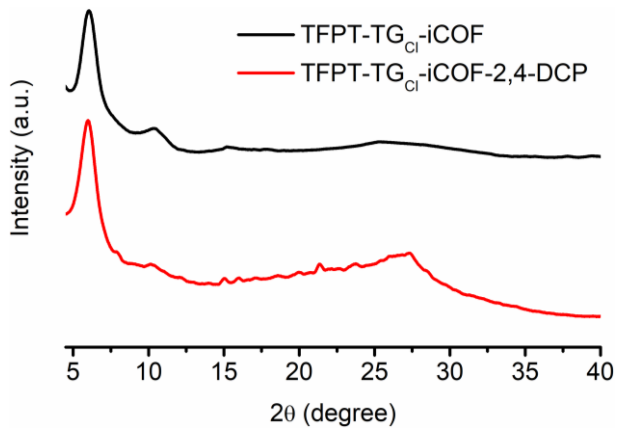

Figure S28. PXRD patterns of TFPT-TG$_{Cl}$-iCOF before and after 2,4-DCP adsorption.

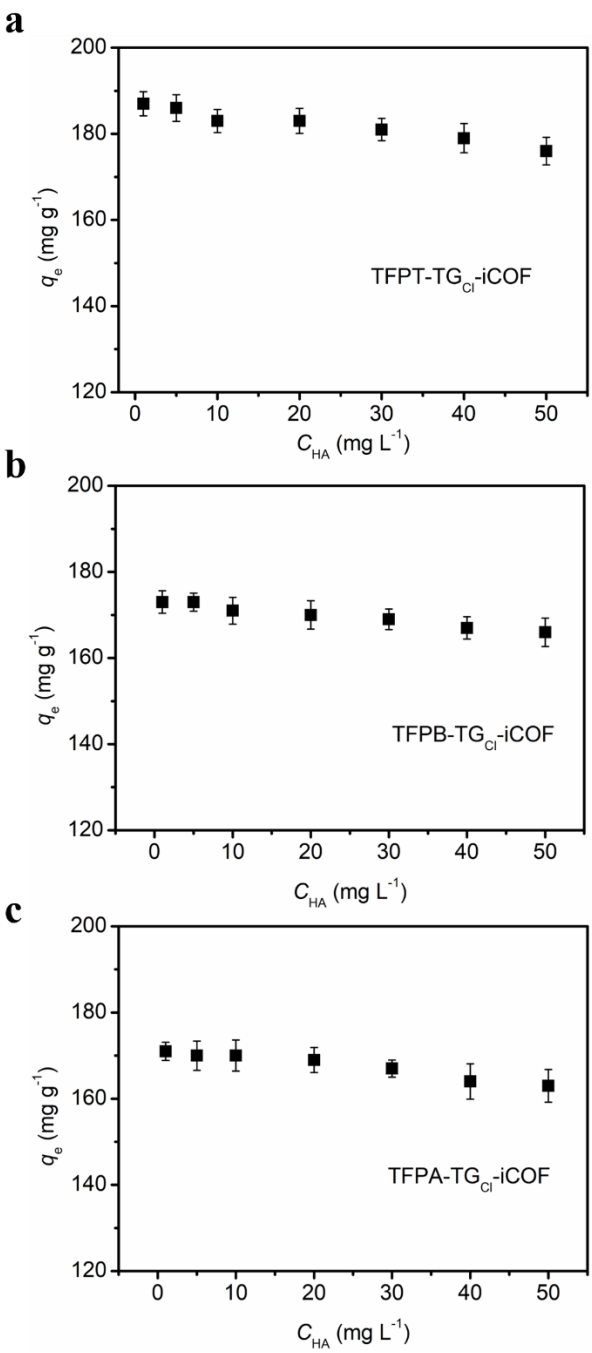

Figure S29. Effect of HA on the adsorption capacity of 2,4-DCP (200 mg L^{-1}) on (a) TFPT-TG_{Cl}-iCOF, (b) TFPB-TG_{Cl}-iCOF and (c) TFPA-TG_{Cl}-iCOF at 25 ^{o}C.

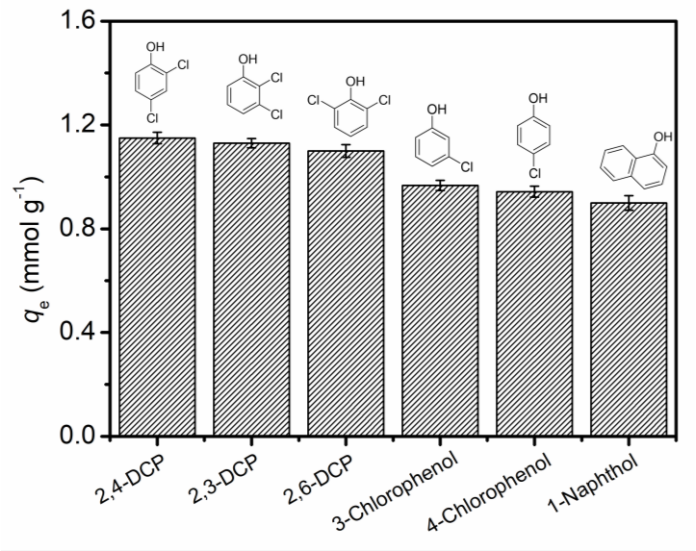

Figure S30. Adsorption of various organic pollutants on TFPT-TG_{Cl}-iCOF with initial concentration of 1.2 mmol L^{-1} at 25 ^{o}C.

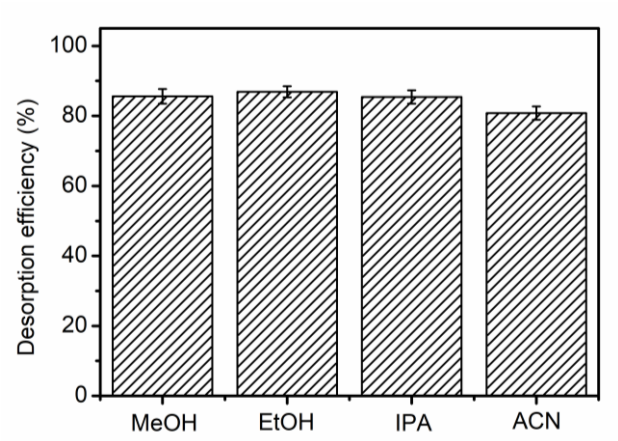

Figure S31. Effect of eluents (1 mL) on the desorption efficiency of 2,4-DCP from TFPT-TG_{Cl}-iCOF (elution time: 10 min).

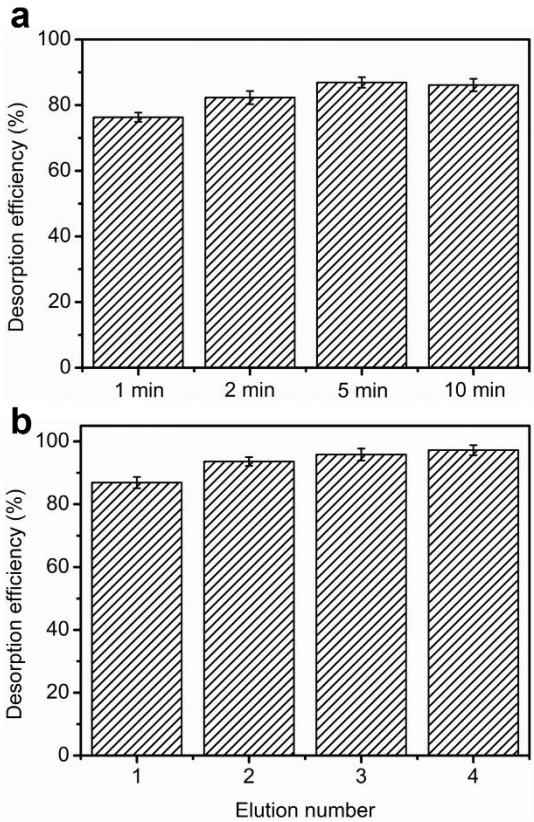

Figure S32. Effects of: (a) elution time and (b) elution number on the desorption of 2,4-DCP from TFPT-TG_{Cl}-iCOF (1 mg) by using EtOH (1 mL) as the eluent.

Supplementary Tables

Table S1. Comparison of the density of cationic charges for three iCOFs

Name	TFPT-TG_{Cl}-iCOF	TFPB-TG_{Cl}-iCOF	TFPA-TG_{Cl}-iCOF
Simplest formula of a HU[a]	$C_{25}H_{18}N_9Cl$	$C_{28}H_{21}N_6Cl$	$C_{22}H_{18}N_7Cl$
Molecular weight of a HU (g mol^{-1})	479.5	476.5	415.5
Cationic-charge number of a HU	1[b]	1	1
Density of cationic charge (mmol g^{-1})	2.086	2.099	2.407

a: HU is the abbreviation of hexagonal unit

b: There are three cationic guanidine-based charge in a HU, and one charge is shared by three HUs. So, there is one net cationic charge in a HU.

Table S2. Fractional atomic coordinates for the unit cell of TFPT-TG_{Cl}-iCOF after Pawley refinement

TFPT-TG_{Cl}-iCOF in slipped model			
TFPT-TG_{Cl}-iCOF [a]: Space group symmetry P6 a = b = 17.49 Å, c = 3.496 Å, α = β =90° and γ = 120° Rwp = 3.37%, Rwp (w/o, bck) = 2.73%, Rp = 1.28%			
Atom	x	y	z
N1	0.20784	-0.18563	-0.00000
C2	0.24089	-0.24127	0.00000
N3	0.33031	-0.20795	0.00000
N4	0.25655	-0.09250	-0.00000
N5	0.09080	-0.37517	0.00000
N6	0.18446	-0.33028	0.00000
N7	0.37503	-0.25617	0.00000
C8	0.33566	-0.34163	-0.00000
C9	0.38606	-0.38775	-0.00000
C10	0.47914	-0.34126	-0.00000
C11	0.52549	-0.38699	-0.00000
C12	0.47935	-0.47958	-0.00000
C13	0.38630	-0.52574	-0.00000
C14	0.33993	-0.48003	0.00000
N15	0.48060	-0.62261	0.00000
C16	0.52785	-0.52806	0.00000
N17	0.61783	-0.48411	-0.00000
C18	0.66256	-0.52894	0.00000
C19	0.52672	-0.66583	0.00000
C20	0.47923	-0.76311	0.00000
C21	0.76042	-0.48018	-0.00000
N22	0.61695	-0.61881	0.00000
C23	0.38615	-0.81155	0.00000
C24	0.80778	-0.38758	-0.00000
C25	0.52643	-0.80833	0.00000
C26	0.48121	-0.90063	-0.00000
C27	0.38842	-0.94865	-0.00000
C28	0.34096	-0.90376	-0.00000
C29	0.80729	-0.52574	-0.00000
C30	0.90009	-0.47937	-0.00000
C31	0.94702	-0.38682	-0.00000
C32	0.90055	-0.34121	0.00000
C33	0.04427	-0.33637	0.00000

C34	0.34249	-0.04535	-0.00000
H35	0.37627	-0.13540	0.00000
H36	0.21962	-0.36826	0.00000
H37	0.26004	-0.38274	-0.00000
H38	0.51718	-0.26597	-0.00000
H39	0.60120	-0.34865	-0.00000
H40	0.34799	-0.60104	0.00000
H41	0.26422	-0.51802	0.00000
H42	0.34689	-0.77568	0.00000
H43	0.77058	-0.34965	0.00000
H44	0.60213	-0.76937	0.00000
H45	0.52003	-0.93694	-0.00000
H46	0.26526	-0.94252	-0.00000
H47	0.76926	-0.60103	-0.00000
H48	0.93777	-0.51682	-0.00000
H49	0.93833	-0.26592	0.00000
H50	0.07897	-0.26118	-0.00000
H51	0.38385	-0.07903	-0.00000
H52	0.13632	0.79383	0.00000
Cl53	0.17349	0.93394	1.00000

a: The symmetric space group of TFPT-TG_{Cl}-iCOF without chloride anions was P6. After adding a chloride atom to each TG_{Cl} fragment, the symmetry of unit cell was turned into P1.

Table S3. Fractional atomic coordinates for the unit cell of TFPB-TG_{Cl}-iCOF after Pawley refinement

TFPB-TG_{Cl}-iCOF in slipped model			
TFPB-TG_{Cl}-iCOF [b]: Space group symmetry P6 a = b = 17.55 Å, c = 3.504 Å, α = β =90°, γ = 120° Rwp = 4.93%, Rwp (w/o, bck) = 11.81%, Rp = 2.23%			
Atom	x	y	z
N1	0.22663	-0.18623	-0.00000
C2	0.25937	-0.24208	-0.00000
N3	0.34797	-0.20935	0.00000
N4	0.27505	-0.09344	-0.00000
N5	0.11072	-0.37505	-0.00000
N6	0.20351	-0.33068	-0.00000
N7	0.39233	-0.25777	0.00000
C8	0.35345	-0.34293	0.00000
C9	0.40366	-0.38909	0.00000
C10	0.49583	-0.34291	-0.00000
C11	0.54209	-0.38855	-0.00000
C12	0.49700	-0.48093	-0.00000
C13	0.40460	-0.52662	-0.00000
C14	0.35831	-0.48099	-0.00000
C15	0.50101	-0.62156	0.00000
C16	0.54602	-0.52933	0.00000
C17	0.63826	-0.48372	-0.00000
C18	0.68547	-0.52874	-0.00000
C19	0.54662	-0.66819	0.00000
C20	0.49822	-0.76561	-0.00000
C21	0.78289	-0.47971	-0.00000
C22	0.63885	-0.62097	-0.00000
C23	0.40584	-0.81290	-0.00000
C24	0.82960	-0.38732	0.00000
C25	0.54391	-0.81231	-0.00000
C26	0.49827	-0.90423	-0.00000
C27	0.40637	-0.95079	0.00000
C28	0.36019	-0.90480	-0.00000
C29	0.83018	-0.52481	0.00000
C30	0.92209	-0.47854	0.00000
C31	0.96808	-0.38637	-0.00000
C32	0.92152	-0.34103	0.00000
C33	0.06444	-0.33617	-0.00000

C34	0.36022	-0.04715	0.00000
H35	0.39350	-0.13712	0.00000
H36	0.23843	-0.36878	-0.00000
H37	0.27854	-0.38365	0.00000
H38	0.53326	-0.26789	-0.00000
H39	0.61710	-0.35016	-0.00000
H40	0.36668	-0.60164	-0.00000
H41	0.28330	-0.51876	-0.00000
H42	0.42600	-0.65996	0.00000
H43	0.67486	-0.40872	-0.00000
H44	0.67724	-0.65758	-0.00000
H45	0.36744	-0.77629	-0.00000
H46	0.79250	-0.34940	0.00000
H47	0.61892	-0.77454	-0.00000
H48	0.53605	-0.94148	-0.00000
H49	0.28518	-0.94239	-0.00000
H50	0.79293	-0.59982	0.00000
H51	0.95985	-0.51580	0.00000
H52	0.95853	-0.26602	0.00000
H53	0.09864	-0.26125	-0.00000
H54	0.40094	-0.08135	0.00000
H55	0.16382	0.81465	1.00000
Cl56	0.19269	0.93343	1.00000

b: The symmetric space group of TFPB-TG_{Cl}-iCOF without chloride anions was P6. After adding chloride atoms to each TG_{Cl} fragment, the symmetry of unit cell was turned into P1.

Table S4. Fractional atomic coordinates for the unit cell of TFPA-TG_{Cl}-iCOF after Pawley refinement

TFPA-TG_{Cl}-iCOF in slipped model			
TFPA-TG_{Cl}-iCOF [c]: Space group symmetry P6 a = b = 15.00 Å, c = 3.756 Å, α = β =90°, γ = 120° Rwp = 8.42%, Rwp (w/o, bck) = 19.73%, Rp = 6.35%			
Atom	x	y	z
N1	0.23499	-0.20475	0.15512
C2	0.27474	-0.26877	0.14584
N3	0.37851	-0.22901	0.15512
N4	0.29115	-0.09638	0.13908
N5	0.10236	-0.42474	0.13908
N6	0.21073	-0.37253	0.15512
N7	0.43072	-0.28518	0.13909
C8	0.38955	-0.37877	0.02167
C9	0.44699	-0.43407	0.01615
C10	0.54617	-0.39055	0.15989
C11	0.59852	-0.44565	0.15693
C12	0.55353	-0.54470	0.00700
C13	0.45417	-0.58700	-0.13876
C14	0.40115	-0.53252	-0.13220
C15	0.45163	-0.76810	0.15692
C16	0.55067	-0.71404	0.00700
N17	0.60807	-0.60210	0.00477
C18	0.72002	-0.54756	0.00700
C19	0.77408	-0.59254	0.15692
C20	0.59297	-0.77110	-0.13874
C21	0.39652	-0.87556	0.15988
C22	0.44004	-0.93122	0.01615
C23	0.53850	-0.87860	-0.13218
C24	0.88154	-0.54019	0.15989
C25	0.93720	-0.44101	0.01615
C26	0.88457	-0.39518	-0.13220
C27	0.77707	-0.44820	-0.13876
C28	0.04993	0.61643	0.02167
C29	0.38475	0.95605	0.02168
H30	0.43057	-0.14457	0.17731
H31	0.25165	-0.41679	0.17763
H32	0.30689	-0.41984	-0.08027
H33	0.58435	-0.30996	0.27968

H34	0.67883	-0.40927	0.27832
H35	0.41579	-0.66683	-0.26458
H36	0.32023	-0.56845	-0.24818
H37	0.41524	-0.72418	0.27830
H38	0.73016	-0.67285	0.27832
H39	0.67281	-0.72965	-0.26455
H40	0.31593	-0.91797	0.27966
H41	0.57464	-0.92337	-0.24838
H42	0.92395	-0.57837	0.27968
H43	0.92934	-0.31427	-0.24840
H44	0.73435	-0.41099	-0.26350
H45	0.09152	0.69908	-0.08026
H46	0.42581	0.91446	-0.08025
H47	0.14959	0.75488	0.15511
Cl48	0.17302	0.89779	0.13906

c: The symmetric space group of original TFPA-TG_{Cl}-iCOF without chloride anions was P6. After adding chloride atoms to each TG_{Cl} fragment, the symmetry of unit cell was turned into P1.

Table S5. Parameters of the Langmuir models for the adsorption of 2,4-DCP on the iCOFs under different temperatures

	T (K)	q_0 (mg g^{-1})	b (L mg^{-1})	R^2
TFPT-TG$_{Cl}$-iCOF	298	892.9 ± 4.3	0.0170 ± 0.0013	0.9961
	308	943.4 ± 3.1	0.0181 ± 0.0031	0.9955
	318	1010.3 ± 4.0	0.0195 ± 0.0022	0.9961
	328	1079.1 ± 3.4	0.0229 ± 0.0018	0.9970
TFPB-TG$_{Cl}$-iCOF	298	578.0 ± 5.1	0.0157 ± 0.0014	0.9969
	308	609.8 ± 3.6	0.0167 ± 0.0026	0.9945
	318	649.4 ± 4.6	0.0180 ± 0.0011	0.9925
	328	684.9 ± 3.8	0.0208 ± 0.0027	0.9943
TFPA-TG$_{Cl}$-iCOF	298	467.3 ± 5.6	0.0188 ± 0.0032	0.9958
	308	495.1 ± 3.6	0.0235 ± 0.0028	0.9972
	318	534.8 ± 4.2	0.0280 ± 0.0017	0.9976
	328	574.7 ± 3.9	0.03518 ± 0.0021	0.9982

Table S6. Comparison of the adsorption capacities of various adsorbents for 2,4-DCP removal

Adsorbents	q_0[a] (mg g^{-1})	Conditions	Refs
KOH activated carbon (KOH / char 3.0)	728	T = 30 ^{o}C	[S7]
Carbon nanotubes/porous polyimide composites (1/1)	506	T = 25 ^{o}C	[S8]
Activated carbon fiber	372	T = 20 ^{o}C	[S9]
Activated carbon AP-42	339	T = 25 ^{o}C	[S10]
Organobentonite	282	T = 30 ^{o}C	[S11]
Mn modified polygonum orientale linn derived activated carbon	244	pH = 5.0, T = 25 ^{o}C	[S12]
Empty fruit bunch derived active carbon	233	T = 25 ^{o}C	[S13]
Fe_3O_4@C	149	pH = 11.0, T = 25 ^{o}C	[S14]
Cattail fiber activated carbon	143	T = 20 ^{o}C	[S15]
Banana pitch carbon	129	pH = 2.0, T = 30 ^{o}C	[S16]
Carbon dots-mesoporous organosilica	100	pH = 7.0, T = 35 ^{o}C	[S17]
Cyclodextrin-ionic liquid polymer (CD-BIMOTs-TDI)	71	T = 25 ^{o}C	[S18]
TFPT-TG_{Cl}-iCOF	**893**	pH = 7.0, T = 25 ^{o}C	**This work**
TFPB-TG_{Cl}-iCOF	**685**		
TFPA-TG_{Cl}-iCOF	**575**		

a: Saturated adsorption capacities of different adsorbents.

Table S7. Thermodynamic parameters of Langmuir model for the adsorption of 2,4-DCP on TFPT-TG_{Cl}-iCOF, TFPB-TG_{Cl}-iCOF and TFPA-TG_{Cl}-iCOF under various temperatures

	ln K_0	ΔG (kJ mol^{-1})	T (K)	ΔH (kJ mol^{-1})	ΔS (J mol^{-1} K^{-1})
TFPT-TG_{Cl}-iCOF	3.318	-8.2	298	10.1	61.4
	3.434	-8.8	308		
	3.548	-9.4	318		
	3.695	-10.1	328		
TFPB-TG_{Cl}-iCOF	2.863	-7.1	298	19.4	88.7
	3.077	-7.9	308		
	3.346	-8.8	318		
	3.569	-9.7	328		
TFPA-TG_{Cl}-iCOF	3.295	-8.1	298	26.4	115.9
	3.588	-9.3	308		
	3.905	-10.4	318		
	4.276	-11.6	328		

Table S8. Kinetic parameters for the adsorption of 2,4-DCP on TFPT-TG_{Cl}-iCOF, TFPB-TG_{Cl}-iCOF and TFPA-TG_{Cl}-iCOF at 298 K

	C_0[a] (mg L^{-1})	q_e (exp)[b] (mg g^{-1})	q_e (cal)[c] (mg g^{-1})	k_2[d] (g mg^{-1} min^{-1})	R^2
TFPT-TG_{Cl}-iCOF	50	47.9 ± 1.1	48.0 ± 1.4	2.85×10^{-1}	0.9999
	100	95.1 ± 1.3	95.5 ± 2.1	1.74×10^{-1}	0.9999
	200	187.2 ± 2.0	187.6 ± 2.7	6.43×10^{-2}	0.9999
	400	357.4 ± 3.3	358.4 ± 3.5	1.44×10^{-2}	0.9999
	600	501.7 ± 3.9	507.6 ± 4.2	3.13×10^{-3}	0.9999
TFPB-TG_{Cl}-iCOF	50	46.4 ± 1.3	46.6 ± 1.8	1.36×10^{-1}	0.9999
	100	91.6 ± 1.0	91.9 ± 2.1	7.37×10^{-2}	0.9998
	200	173.4 ± 2.5	173.6 ± 2.7	1.78×10^{-2}	0.9999
	400	305.8 ± 3.1	306.8 ± 3.4	3.09×10^{-3}	0.9997
	600	401.3 ± 3.0	398.4 ± 4.2	4.85×10^{-4}	0.9999
TFPA-TG_{Cl}-iCOF	50	47.4 ± 1.2	47.6 ± 1.6	1.11×10^{-1}	0.9998
	100	92.2 ± 1.4	92.3 ± 2.1	3.92×10^{-2}	0.9999
	200	172.5 ± 3.9	172.7 ± 3.1	8.84×10^{-3}	0.9999
	400	281.1 ± 2.6	284.9 ± 2.6	9.71×10^{-4}	0.9997
	600	350.6 ± 3.7	350.9 ± 3.1	7.42×10^{-5}	0.9999

a: Initial concentrations of 2,4-DCP.

b: Adsorption capacities at equilibrium from experiments.

c: Adsorption capacities at equilibrium from calculations.

d: Rate constants for pseudo-second-order adsorption.

Table S9. Comparison of the adsorption kinetics of various adsorbents for 2,4-DCP

Adsorbents	k (g mg^{-1} min^{-1})[a]	C_0 (mg L^{-1})[b]	Refs
Empty fruit bunch derived active carbon	1.9×10^{-1}	50	[S13]
Ammonia modified activated carbon	1.7×10^{-1}	50	[S19]
Palm pith carbon	1.2×10^{-2}	40	[S20]
non-living mycelial pellets	9.4×10^{-2}	52	[S21]
Cyclodextrin-ionic liquid polymer (CD-BIMOTs-TDI)	7.5×10^{-2}	--	[S17]
Cattail fiber AC	6.5×10^{-3}	50	[S14]
Mn modified polygonum orientale linn derived activated carbon	4.4×10^{-3}	100	[S11]
Organobentonite	2.2×10^{-3}	70	[S10]
Banana pitch carbon	1.3×10^{-3}	100	[S15]
Carbon dots-mesoporous organosilica	7.9×10^{-4}	100	[S16]
Activated carbon fiber	3.9×10^{-5}	326	[S9]
TFPT-TG$_{Cl}$-iCOF	**2.85×10^{-1}**	**50**	**This work**
	1.33×10^{-1}	**100**	

a: Adsorption kinetics rate constants of adsorbents calculated from pseudo-second-order kinetics model.

b: Initial concentrations of 2,4-DCP.

References

[S1] Frisch, M. J.; Trucks, G. W.; Schlegel, H. B.; Scuseria, G. E.; Robb, M. A.; Cheeseman, J. R.; Scalmani, G.; Barone, V.; Petersson, G. A.; Nakatsuji, H.; Li, X.; Caricato, M.; Marenich, A.; Bloino, J.; Janesko, B. G.; Gomperts, R.; Mennucci, B.; Hratchian, H. P.; Ortiz, J. V.; Izmaylov, A. F.; Sonnenberg, J. L.; Williams-Young, D.; Ding, F.; Lipparini, F.; Egidi, F.; Goings, J.; Peng, B.; A. Petrone,; Henderson, T.; Ranasinghe, D.; Zakrzewski, V. G.; Gao, J.; Rega, N.; Zheng, G.; Liang, W.; Hada, M.; Ehara, M.; Toyota, K.; Fukuda, R.; Hasegawa, J.; Ishida, M.; Nakajima, T.; Honda, Y.; Kitao, O.; Nakai, H.; Vreven, T.; Throssell, K.; Montgomery, J. A.; Peralta, Jr., J. E.; Ogliaro, F.; Bearpark, M.; Heyd, J. J.; Brothers, E.; Kudin, K. N.; Staroverov, V. N.; Keith, T.; Kobayashi, R.; Normand, J.; Raghavachari, K.; Rendell, A.; Burant, J. C.; Iyengar, S. S.; Tomasi, J.; Cossi, M.; Millam, J. M.; Klene, M.; Adamo, C.; Cammi, R.; Ochterski, J. W.; Martin, R. L.; Morokuma, K.; Farkas, O.; Foresman, J. B.; Fox, D. J. Gaussian, Inc., Wallingford CT, 2016.

[S2] Becke, A. D. Density-functional thermochemistry. III. The role of exact exchange. *J. Chem. Phys*. **1993**, *98*, 5648-5652.

[S3] Lee, C.; Yang, W.; Parr, R. G. Development of the colle-salvetti correlation-energy formula into a functional of the electron density. *Phys. Rev. B.* **1988**, *37*, 785-789.

[S4] Perdew, J. P.;, Burke, K.; Ernzerhof, M. Generalized gradient approximation made simple. *Phys. Rev. Let.* **1996**, *77*, 3865-3868.

[S5] Grimme, S.; Antony, J.; Ehrlich, S. A consistent and accurate ab initio parametrization of density functional dispersion correction (DFT-D) for the 94 elements H-Pu. *J. Chem. Phys*. **2010**, *132*, 154104.

[S6] Halder, A.; Kandambeth, S.; Biswal, B. P.; Kaur, G.; Roy, N. C.; Addicoat, M.; Salunke, J. K.; Banerjee, S.; Vanka, K.; Heine, T.; Verma, S.; Banerjee, R. Decoding the morphological diversity in two dimensional crystalline porous polymers by core planarity modulation. *Angew. Chem. Int. Ed*. **2016**, *55*, 7806-7810.

[S7] Wu, F. C.; Tseng, R. L.; Hu, C. C. Comparisons of pore properties and adsorption performance of KOH-activated and steam-activated carbons. *Micropor. Mesopor. Mat*. **2005**, *80*, 95-106.

[S8] Yuan, H.; You, Q. L; Song, L. J.; Liao, G. Y. Xia, H.; Wang, D. S. Preparation of carbon nanotubes/porous polyimide composites for effective adsorption of 2,4-dichlorophenol. *RSC Adv*. **2016**, *6*, 95825-95835.

[S9] Wang, J. P.; Feng, H. M.; Yu, H. Q. Analysis of adsorption characteristics of 2,4-dichlorophenol from aqueous solutions by activated carbon fiber. *J. Hazard. Mater*. **2007**, *144*, 200-207.

[S10] Daifullah, A. A. M.; Girgis, B. S. Removal of some substituted phenols by activated carbon obtained from agricultural waste. *Water Res*. **1998**, *32*, 1169-1177.

[S11] Zhou, Y.; Jin, X. -Y.; Lin, H.; Chen, Z. -L. Synthesis, characterization and potential application of organobentonite in removing 2,4-DCP from industrial wastewater. *Chem. Eng. J*. **2011**,*166*, 176-183.

[S12] Wang, L.; Zhang, J.; Zhao, R.; Zhang, C.; Li, C.; Li, Y. Adsorption of 2,4-dichlorophenol on Mn-modified activated carbon prepared from polygonum orientale linn. *Desalination.* **2011**, *266*, 175-181.

[S13] Shaarani, F. W.; Hameed, B. H. Batch adsorption of 2,4-dichlorophenol onto activated carbon derived from agricultural waste. *Desalination*. **2010**, *255*, 159-164.

[S14] Wang, L.; Gan, K.; Lu, D.; Zhang, J. Hydrophilic Fe_3O_4 @ C for high-capacity adsorption of

2,4-dichlorophenol**.** *Eur. J. Inorg. Chem.* **2016**, 890-896.

[S15] Ren, L.; Zhang, J.; Li, Y.; Zhang, C. Preparation and evaluation of cattail fiber-based activated carbon for 2,4-dichlorophenol and 2,4,6-trichlorophenol removal. *Chem. Eng. J*. **2011**, 168, 553–561.

[S16] Sathishkumar, M.; Vijayaraghavan, K.; Binupriya, A. R.; Stephan, A. M.; Choi, J. G.; Yun, S. E. Porogen effect on characteristics of banana pith carbon and the sorption of dichlorophenols. *J. Colloid. Interf. Sci.* **2008**, *320*, 22-29.

[S17] Wang, L. Cheng, C. Tapas, S.; Lei, J.; Matsuoka, M.; Zhang. J.; Zhang, F. Carbon dots modified mesoporous organosilica as an adsorbent for the removal of 2, 4-dichlorophenol and heavy metal ions. *J. Mater. Chem. A*. **2015**, *3*, 13357-13364.

[S18] Raoov, M.; Mohamad, S.; Abas, M. R. Removal of 2,4-dichlorophenol using cyclodextrin-ionic liquid polymer as a macroporous material: characterization, adsorption isotherm, kinetic study, thermodynamics. *J. Hazard. Mater.* **2013**, *263*, 501-516.

[S19] Shaarani, F.W.; Hameed, B.H. Ammonia-modified activated carbon for the adsorption of 2,4-dichlorophenol. *Chem. Eng. J.* **2011**, *169*, 180-185.

[S20] Sathishkumar, M.; Binupriya, A.R.; Kavitha, D. S.; Yun, E. Kinetic and isothermal studies on liquid-phase adsorption of 2,4-dichlorophenol by palm pith carbon. *Bioresource Technol*. **2007**, *98*, 866–873.

[S21] Wu, J. Yu, H. -Q. Biosorption of 2,4-dichlorophenol from aqueous solution by Phanerochaete chrysosporium biomass: Isotherms, kinetics and thermodynamics. *J. Hazard. Mater.* **2006**, *137* 498–508.